A Novel BST@TPU Membrane with Superior UV Durability for Highly Efficient Daytime Radiative Cooling

Submitted version of the paper: "A Novel BST@TPU Membrane with Superior UV Durability for Highly Efficient Daytime Radiative Cooling"

Published version available at:
X. Li, L. Pattelli, Z. Ding, M. Chen, T. Zhao, Y. Li, H. Xu, L. Pan, J. Zhao, A Novel BST@TPU Membrane with Superior UV Durability for Highly Efficient Daytime Radiative Cooling. *Adv. Funct. Mater.* 2024, 34, 2315315. https://doi.org/10.1002/adfm.202315315

A Novel BST@TPU Membrane with Superior UV Durability for Highly Efficient Daytime Radiative Cooling

Xin Li [a], *Lorenzo Pattelli* [b, c] *Zhenmin Ding* [a], *Mingjun Chen* [a], *Tao Zhao* [d], *Yao Li* [d, e], *Hongbo Xu* [a, *], *Lei Pan* [a, *], *Jiupeng Zhao* [a, *]

X. Li, Z. Ding, M. Chen, Prof. J. Zhao, Dr. L. Pan, Prof. H. Xu
School of Chemistry and Chemical Engineering, Harbin Institute of Technology, Harbin, 150001, PR China
E-mail: iamxhb@hit.edu.cn, panlei@hit.edu.cn, jpzhao@hit.edu.cn

Dr. L. Pattelli
Istituto Nazionale di Ricerca Metrologica (INRiM), Turin, 10135, Italy
European Laboratory for Non-linear Spectroscopy (LENS), Sesto Fiorentino, 50019, Italy

Prof. Y. Li, T. Zhao
Center for Composite Materials and Structure, Harbin Institute of Technology, Harbin, 150001, China

Keywords: daytime radiative cooling, UV durability, coaxial electrospinning, barium strontium titanate, thermoplastic polyurethane

Abstract

Passive radiative cooling technologies play an integral role in advancing sustainable development. While the potential of polymer-based radiative cooling materials is increasingly recognized, they often degrade under prolonged UV radiation exposure, which undermins both their mechanical and radiative cooling performance. To address this challenge, we employ a coaxial electrospinning method to prepare a BST@TPU membrane, with a core layer of strontium barium titanate nanorods (BST NRs) and a shell layer of thermoplastic polyurethane (TPU). Capitalizing on the UV absorption and free radical adsorption properties of BST NRs, the UV stability of the TPU membrane is significantly increased. Additionally, the inclusion of high refractive index BST NRs compensates for the decrease in reflectivity caused by their UV absorption. After 216 h of continuous 0.7 kW m^{-2} UV irradiation, the BST@TPU membrane, which initially exhibits a reflectance of 97.2%, demonstrated a modest decline to 92.1%. Its net radiative cooling power maintains 85.78 W m^{-2} from the initial of 125.21 W m^{-2}, extending the useful lifetime of the TPU membrane threefold. This innovation extends promise for enhancing the efficiency and durability of radiative cooling materials, contributing to sustainable cooling solutions across various applications.

1. Introduction

With the escalating global climate change crisis and the growing scarcity of energy resources, the imperative for sustainable solutions grows. [1] Daytime radiative cooling technology, with its potential in energy-saving, is gaining significant traction in response. [2] For polymer-based radiative cooling materials aiming to integrate high reflectivity and high emissivity, [3] achieving this functionality requires a twofold approach. One is the strategic integration of high-absorption functional groups in the atmospheric transparency window, notably C−O, C−H, and C−O−C. [4] The other is the careful engineering of nanoscale configurations yielding multiple refractive index discontinuities, facilitating enhanced scattering of incident solar radiation. [5] Among various candidates,[3b] thermoplastic polyurethane (TPU)-based radiative cooling materials emerge as noteworthy candidates, offering both suitable functional groups and straightforward fabrication strategies which have already yielded pioneering advancements in energy efficacy and eco-sustainability. [6] The versatility of TPU extend its applicability to

diverse domains, including construction [6b] clothing materials [7], thereby promoting the practical implementation of radiative cooling concepts.

A significant challenge associated with many polymer-based radiative cooling materials, including TPU, lies in their environmental stability [8]. Prolonged UV absorption by polymers can lead to the degradation of their chemical bonds, [9] resulting in yellowing of the polymer. Moreover, the potential reduction in cooling performance due to the increased visible light absorption, [8a, 10] which brings difficulty to the popularization of large-scale radiative cooling polymer. Conventional UV blockers, such as carbon black [11] and commercial organic UV absorbers [9d, 12] are not viable options for radiative cooling polymer, as these additives could result in broad spectral absorption of sunlight, making it difficult to meet the premise of low absorption for radiative cooling materials. Bolstering the UV aging resistance of polymer materials without compromising its radiative cooling efficacy involves a dedicate tradeoff. Integrating inorganic nanoparticles into a polymer matrix can enhance its reflection or absorption of UV radiation. [9a] Commonly considered as the UV reflectors, Al_2O_3 [2d, 8e, 13] and $BaSO_4$ [14] possess sufficient bandgap width to suppress solar absorption and relatively high refractive index for effective sunlight scattering.[14b] However, when these particles are mixed with a polymer, the resulting radiative cooling material still exhibits the intrinsic absorption of the polymer in the reflection spectrum, limiting its ability to effectively reflect UV radiation. [15] In contrast, UV absorbing fillers, such as TiO_2 [1d, 8a, 8c, 9d, 16] and ZnO, [17] can better disperse the UV light absorbed by the polymer matrix. Compared with TiO_2 (3.2 eV) [14a] and ZnO (3.3 eV), [17] BST has the bandgap width of approximately 3.04 eV, [18] allowing for a more effective absorption of UV radiation with wavelengths below 408 nm, more accurately covering the wavelengths (< 410 nm) that affect the UV radiation of polymers such as TPU. Integrating UV reflection and absorption nanoparticles can exert their synergistic effect. Li et al. [4b] employed a spray-coating method to overlay TiO_2 nanoparticles as UV absorption layers and Al_2O_3 nanoparticles as UV reflection layers on a polymer film to comprehensively prevent the UV radiation from reaching the polymer matrix. However, the additional inorganic coating may compromise the inherent advantages of the polymer, such as flexibility and mechanical properties. [16b, 19]

The phase separation methods [6a, 6c, 20] and electrospinning methods [6b, 21] are commonly used to prepare flexible polymer-based radiative cooling materials with good mechanical properties. In contrast, electrospinning stands out as a scalable technique that allows for the fabrication of highly reflective materials with exquisite control over nanofiber diameter and distribution. Despite these advancements, organic-inorganic blend fibers prepared by uniaxial spinning often

exhibit uneven particle distribution or bead like morphology, leading to a reduced overall optical reflectivity compared to the anticipated ideal structure from Mie theory. [22] Coaxial electrospinning effectively addresses the challenges of poor dispersion and incompatibility in multi-component materials. [23] By constructing a composite structure of organic shell layer and inorganic core layer, it can ensure a more uniform fiber morphology and even maintain the inherent characteristics of each material. [24] Moreover, nanorods with a high aspect ratio are more prone to orient in an electric field, [25] facilitating their uniform arrangements within the matrix.

Herein, we present a membrane by combining strontium barium titanate nanorods (BST NRs) and thermoplastic polyurethane (TPU) using coaxial electrospinning (BST@TPU membrane). The BST NRs effectively disperse the UV radiation on the TPU, and their high refractive index enhances visible light scattering, counteracting the loss in reflectivity due to UV absorption and thus preserving the high reflectivity of the BST@TPU membrane. Density functional theory (DFT) calculations demonstrate BST NRs can capture free radicals formed during UV aging process of TPU, thereby forestalling aging reactions. Consequently, BST NRs, uniformly distributed within TPU, not only effectively transfer stress to ensure the mechanical properties of the membrane, but also fully utilize the advantages of its optical properties, improving the UV durability of the membrane without compromising its radiative cooling capacity. The reflectivity of the BST@TPU membrane can reach 97.2%, and the emissivity is 93.2%. The UV stability of BST@TPU membrane has been improved to three times than that of TPU membrane. Under 216 h continuous 0.7 kW m^{-2} UV irradiation, the solar reflectance of the BST@TPU membrane only decreased to 92.1% (equivalent to 144 days of outdoor use), which is still associated to a residual cooling power of 85.78 W m^{-2}. In contrast, the TPU membrane would lose its net cooling capacity entirely. This work opens up new avenues for the application of TPU in daytime radiative cooling, and provides a universal strategy for improving the UV stability of polymer-based radiative cooling materials.

2. Results and Discussion

2.1. Design of Radiative Cooling membrane with UV durability

The objective of this study is to improve the UV durability of a TPU membrane while concurrently enhancing its radiative cooling performance, thus the selection of fillers adheres to three main principles. Firstly, to counteract the detrimental effects of UV radiation on the TPU matrix, materials with superior UV absorption should be used. Secondly, preferring materials with a higher refractive index to enhance visible light reflectivity, thereby neutralizing

the decrease in reflectivity caused by UV absorption. Thirdly, the ideal additive should also inhibit the yellowing reaction in TPU membrane (the C−N bond breakage in TPU, and further aging reaction leading to a visible yellow color). [26] BST aligns with the aforementioned design criteria. As illustrated in **Figure 1**a, BST has a refractive index of 2.5 across the entire solar spectrum, which is 1.0 higher than TPU. Additionally, BST exhibits a pronounced extinction coefficient in the UV range, making it attractive for enhancing the UV resistance of TPU. A numerical investigation of the scattering capabilities of BST nanoparticles (BST NPs) (Figure 1b) and BST nanorods (BST NRs) (Figure 1c) were conducted using Mie theory comparing BST NRs against infinite cylinders of equal radius. The diameter range of both was set from 0.1 to 0.4 μm, over a wavelength range of 0.25 to 2.5 μm. Comparative analysis shows that nanorods with identical diameters to BST nanoparticles provide higher scattering across a broader wavelength spectrum. Subsequently, the BST@TPU membrane was fabricated via a two-step electrospinning process (Figure 1d). Firstly, BST NRs are prepared by electrospinning BST sol followed by high-temperature calcination. Then, these nanorods are used as UV absorbing fillers and combined with TPU through coaxial electrospinning. This process can enhance the dispersion of BST NRs in TPU, achieving the ideal uniform fibers that can effectively scatter sunlight. In addition, in combination with the inherent high IR emission ability, the BST@TPU membrane enables daytime radiative cooling.

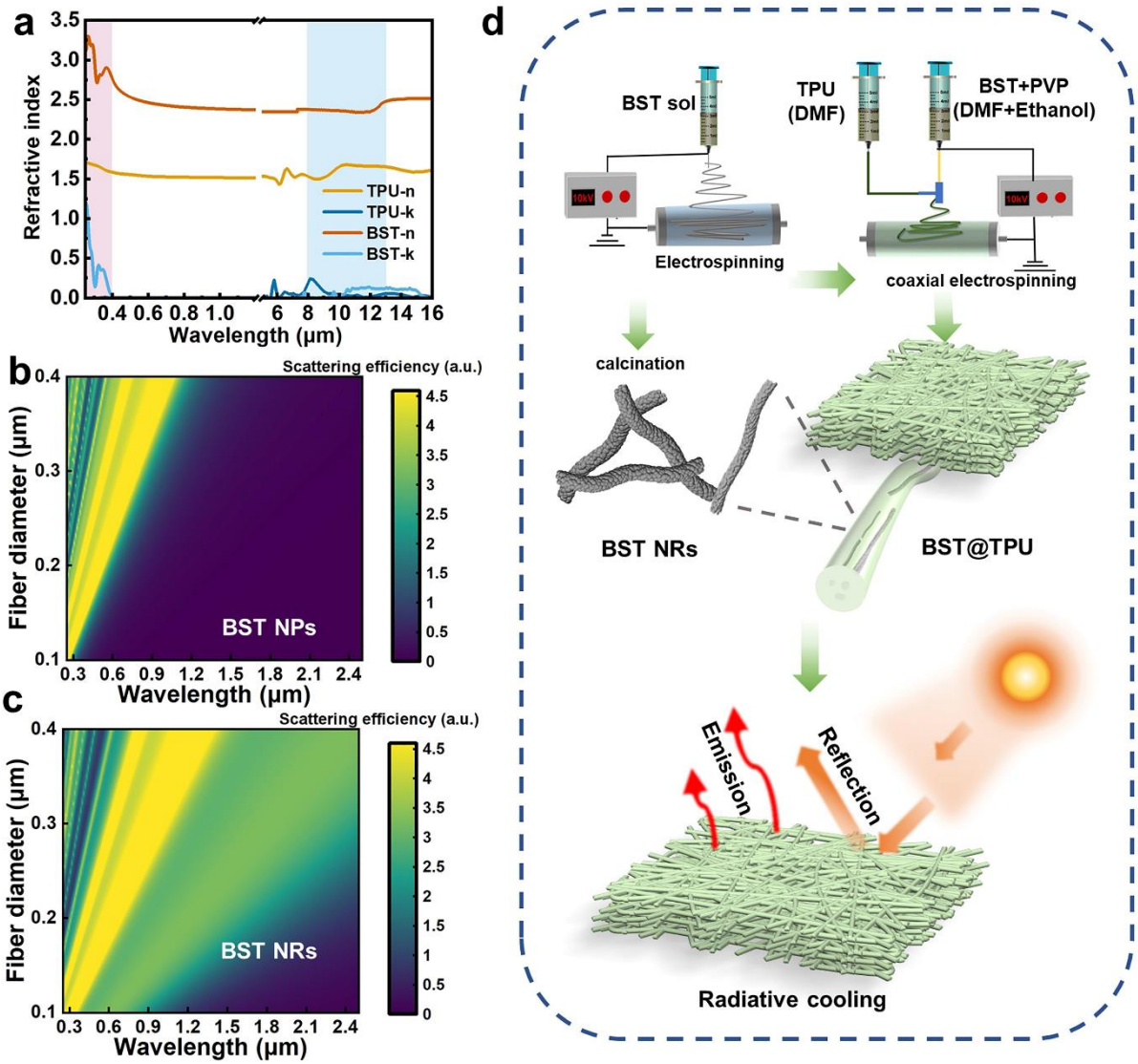

Figure 1. The design, preparation, and radiative cooling performance of the UV durability BST@TPU membrane with core-shell structure. a) The complex spectral refractive index (n + ik) of TPU and BST in the solar and IR wavelength range (0.25 − 16 μm). Simulated scattering efficiency of b) BST NPs and c) BST NRs in the wavelength range of 0.25 − 2.5 μm for fibers with different diameters. d) Schematic diagram for the preparation process of BST@TPU membrane with radiative cooling capability.

2.2. Fabrication of the Radiative Cooling membrane with UV durability

BST NRs were synthesized through electrospinning method followed by subsequent high-temperature calcination (Supplementary Note 1.2). Changes in morphology in Figures S1 (Supporting Information) suggest formation of BST nanorods. The average diameter of the BST NRs was approximately 160 nm (Figure S1c, Supporting Information), with an aspect ratio of 7.9:1 (Figure S1d, Supporting Information). High-temperature calcination ensures the

crystallization of BST (Figure S2a, Supporting Information), which was further confirmed by the observation of distinct lattice fringes in high resolution TEM (HRTEM) images (**Figure 2**a). This crystalline structure is confirmed by the sharp peaks corresponding to $Ba_{0·6}Sr_{0·4}TiO_3$ structures (Figure S2b, Supporting Information). [27] The XPS spectra (Figure S3, Supporting Information) displays peaks corresponding to Ba, Sr, Ti, and O, further corroborating the successful synthesis of BST. [28]

For comparison with the BST@TPU membrane (Supplementary Note 1.3.3), a TPU membrane (Figure 2b, Supplementary Note 1.3.1) and a BST-TPU membrane (Figure 2c, Supplementary Note 1.3.2) were prepared via uniaxial electrospinning. However, the BST-TPU membrane revealed prominent fiber beading caused by the weak interaction and limited coexistence potential between BST NRs and TPU. In contrast, coaxial electrospinning leads to a clearer and more uniform fiber morphology of the BST@TPU membrane (Figure 2d), which is beneficial for ensuring its optical and mechanical properties. For BST@TPU membranes, the core-to-shell spinning speed ratio significantly affects their morphology. [29] A slower core spinning speed could lead to insufficient stretching of the layer, impeding the drawing of uniform and elongated coaxial fibers (Figure S4a, Supporting Information). Increasing the core layer speed from 0.02 mm min^{-1} to 0.08 mm min^{-1} enhanced stretching consistency, fostering a more homogenous fiber morphology. Conversely, excessive core layer speed results in fiber formation instabilities, causing incomplete core coverage (Figure S4b, Supporting Information). All BST@TPU membranes exhibit hydrophobicity (Figure S5, Supporting Information). Therefore, maintaining a balanced core-to-shell spinning speed is crucial for achieving fiber uniformity and stability, which in turn influences the membrane's optical performance.

At a core injection rate of 0.08 mm min^{-1}, BST NRs are uniformly distributed within the TPU matrix, as along with a more ordered interface contact (Figure 2e and Figure 2f), signifying the successful formation of a coaxial structure. Based on these results, the BST@TPU membrane produced with this fabrication parameter is chosen for further tests. The characteristic peaks of BST NRs prove their existence in the composite membrane (Figure 2g). FT-IR spectra emphases the extinction peaks associated with various vibration modes within the atmospheric window are responsible for its high emissivity at infrared wavelengths (Figure 2h). [20-21, 30] XPS analysis further confirms the physical doping of BST NRs into the system (Figure 2i). Figure 2j illustrates that the mechanical properties of TPU depend critically on the uniform dispersion of BST NRs within the TPU matrix. The reduced mechanical performance in the BST-TPU case can be ascribed to the stress concentration associated to the significant fiber beading. Notably, the BST@TPU membrane exhibits an improved Young's modulus enhancement from

3.96 (TPU membrane) to 9.87 MPa, thanks to the effective stress transfer and crack propagation hindrance provided by the uniformly distributed BST NRs, this enhancement contributes to the toughness and durability of the fibers. [9a]

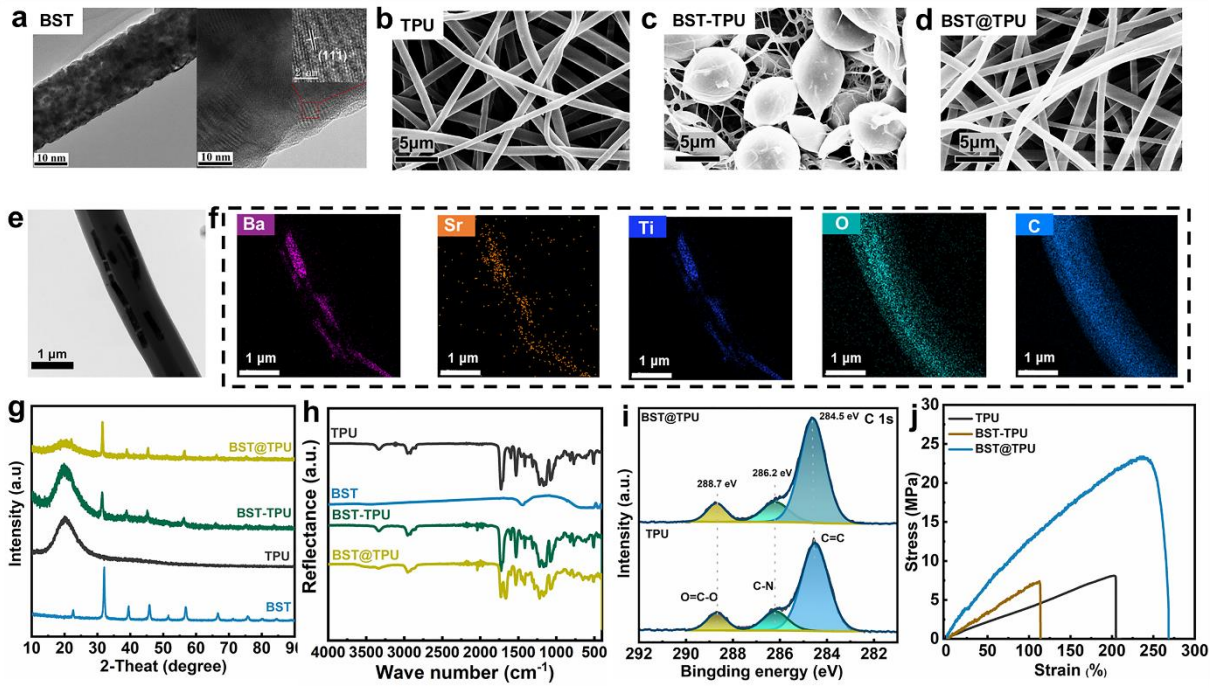

Figure 2. The characterization of BST NRs/TPU composite membrane. a) TEM image and HRTEM image of a single BST NR. SEM images of b) TPU membrane, c) BST-TPU membrane, d) BST@TPU membrane. e) TEM image of a BST@TPU coaxial fiber. f) EDS mapping of Ba, Sr, Ti, O, C elements of the BST@TPU coaxial fiber. g) XRD patterns and h) FT-IR spectra of BST NRs, TPU membrane, BST-TPU membrane and BST@TPU membrane. i) The C1S High resolution XPS (HRXPS) of TPU membrane and BST@TPU membrane. j) Stress-strain curve of the TPU membrane, BST-TPU membrane and BST@TPU membrane.

2.3. Optical Properties of the membranes

The optical properties of the membrane, intricately linked with fiber morphology, are pivotal in defining its radiative cooling capability. [31] As illustrated in Figure S6a (Supporting Information), the BST@TPU membranes prepared with a core layer speed of 0.08 mm min^{-1} exhibits optimal reflectance, positioning it as a prime candidate for radiative cooling applications. A comparative analysis of the reflectance profiles for the three membranes, depicted in **Figure 3**a, indicates that the inclusion of BST NRs indeed augments the UV absorption. However, when compared with the BST-TPU membrane, the BST@TPU membrane displays attenuated UV absorption (Figure S7, Supporting Information) and superior reflectance in the visible light spectrum (500 − 700 nm). As shown in Figure 3c, the integrated

solar reflectance for the TPU membrane, BST-TPU membrane, and BST@TPU membrane are quantified as 95.6%, 93.4%, and 97.2%, respectively (Equation S1, Supporting Information). For BST@TPU membrane, a pronounced scattering effect arises from the uniform dispersion of BST NRs, which can counteract the inherent absorption of BST NRs across UV bands in the BST@TPU membrane. Contrarily, the BST-TPU membrane manifests a distinct bead-like morphology, diverging from the Mie theory and resulting in the inability to harness the refractive index of BST NRs, in turn, resulted in a larger UV absorption and diminished reflectance. In the long-wave infrared range, different preparation processes of the membranes have little effect on their emissivity values. This is attributed to the much larger scale of thermal wavelengths compared to bead size and fiber diameter.[32] The relatively stable absorption characteristics and the limited impact of fiber morphology on its infrared emissivity are confirmed by the minimal alteration in the infrared emissivity of the membranes (Figure 3b and Figure S6b, Supporting Information).

The solar scattering performance of the different fibers can be studied numerically using Mie theory. [5b] The BST@TPU membrane exhibits a significant increase in scattering efficiency within fiber diameters that match visible wavelengths (Figure 3f). Furthermore, it exhibits superior scattering capabilities over a broader wavelength spectrum when compared to TPU fibers (Figure 3d). Conversely, BST-TPU fibers, featuring a higher composite refractive index, experiences a redshift in the effective scattering wavelengths for fibers of equivalent diameter, rendering them less effective in scattering sunlight (Figure 3e). The theoretical net radiative cooling powers at various non-radiative heat transfer coefficients (h_{cc}) relative to conduction and convection under direct sunlight, achieved by the membranes, were calculated using equations reported in Supplementary Note 2.3 at ambient temperature of 303 K. Solar absorption plays a major role in determining radiative cooling efficacy. Although the introduction of BST NRs may increase UV absorption, strategic optimization of the membrane structure can effectively counteract this impact. The BST-TPU membrane, due to its diminished visible light reflectance and augmented UV absorption, achieves a theoretical net radiative cooling power of 81.46 W m^{-2} (Figure 3h), which is notably lower than the 112.81 W m^{-2} of the TPU membrane, which recorded (Figure 3g). Importantly, the excellent optical properties of the BST@TPU membrane endows it with even better radiative cooling performance, reaching a peak value of 125.21 W m^{-2} (Figure 3i). The obtained maximum temperature difference (ΔT) of BST@TPU membrane is progressively reduced to 29.0 °C, 16.4 °C 11.6 °C, 9.1 °C and 7.4 °C with increasing h_{cc} (0 − 12 W m^{-2} K^{-1}). [33] Consequently, experiments aiming

to assess the radiative cooling performance and UV stability were conducted using the BST@TPU membrane, with the TPU membrane as the benchmark.

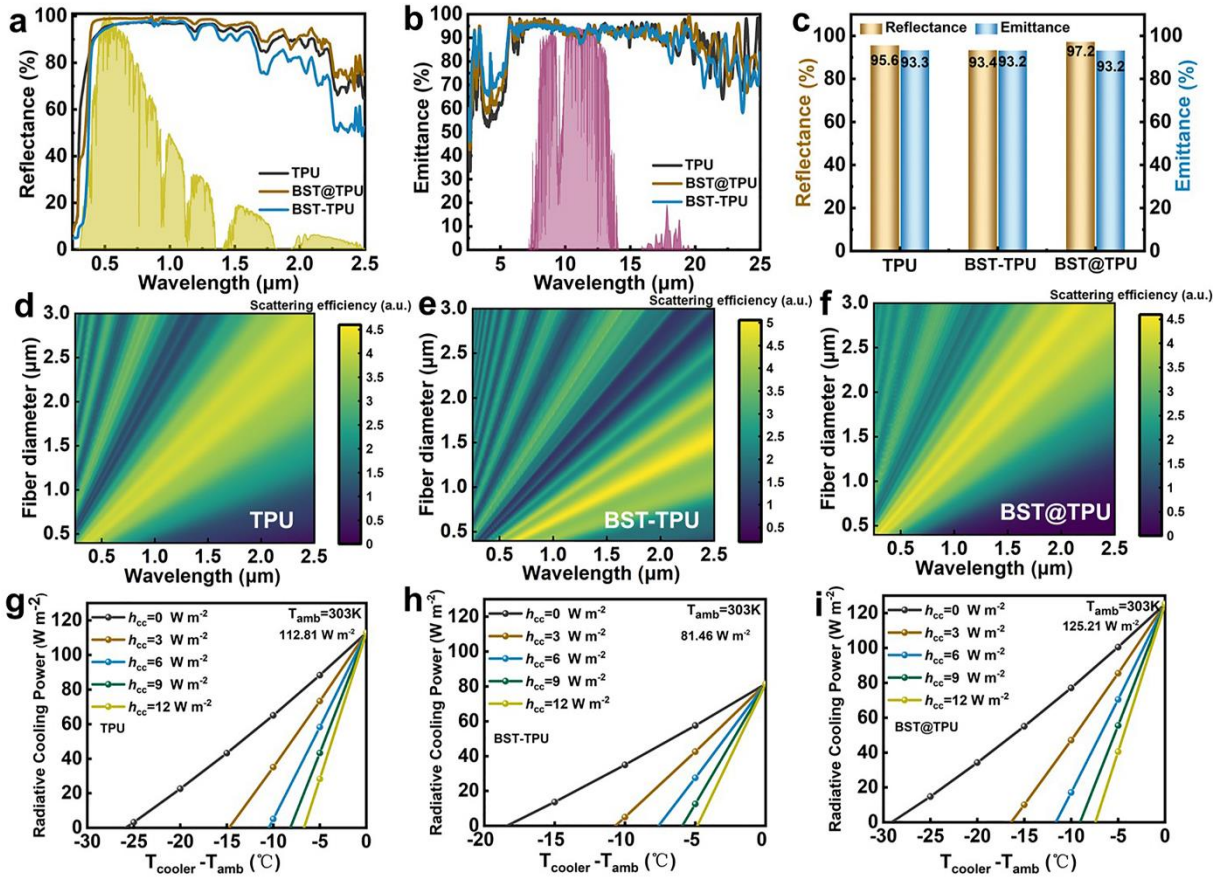

Figure 3. Optical properties of BST NRs/TPU composite membrane. a) UV–vis–NIR reflectance and b) IR emittance of TPU membrane, BST-TPU membrane and BST@TPU membrane presented against the AM1.5 solar spectrum (yellow) and the atmospheric transparency window (pink), respectively. c) The corresponding reflectance and emittance calculation values in Figure 3a and 3b. Simulation of the scattering efficiency of d) TPU fiber, e) BST-TPU fiber and f) BST@TPU fiber across the wavelength range of 0.25 – 2.5 μm with the diameter varied from 0.4 to 3 μm. Theoretical net radiative cooling power of g) TPU membrane, h) BST-TPU membrane, i) BST@TPU membrane under different h_{cc} (0 – 12 W m^{-2}) at T_{amb}=303 K during daytime.

2.4. Radiative Cooling Performance of the membranes

The radiative cooling capabilities of the TPU membrane and BST@TPU membrane were demonstrated through an outdoor cooling test on the eighth-floor rooftop of Harbin Institute of Technology (45°43′49″N, 126°38′11″E) under direct sunlight. The experimental setup is schematically depicted in **Figure 4**a, which includes a polyethylene film closing a polystyrene foam sample box to reduce and stabilize the non-radiative heat exchange terms. The

measurement was conducted under the weather condition of July 21st 2023 (Figure 4b). The real-time sub-ambient temperature and temperature under the membranes' coverage are shown in Figure 4c. The BST@TPU membrane outperforms the TPU membrane in terms of cooling efficiency, with a maximum temperature reduction of 10.3 °C and an average temperature decrease of 6.5 °C during periods of approximately 700 W m^{-2} solar intensity (I_{solar}) from 09:00 to 18:00. In comparison, the TPU membrane exhibits an average temperature drops of 4.3 °C during the same timeframe (Figure 4d). The superior daytime radiative cooling performance of the BST@TPU membrane can be attributed to its higher solar reflectance, which effectively reducing heat gain. Additionally, the decline in the cooling capacity after 15:00 is closely associated with the diminishing solar irradiance and the increased relative humidity. [34] A subsequent experiment was performed by measuring real-time temperature variations inside a metal black car model covered with the BST@TPU membrane, directly exposed to sunlight without any convective shielding (Figure S8a, Supporting Information). Simultaneously, measurements of wind speed, humidity, and solar irradiance on July 20th 2023 were recorded (Figure S8b, Supporting Information). The results revealed that at solar noon, with an average solar intensity of ≈600 W m^{-2}, the average temperature inside the car covered with the BST@TPU membrane is 36.0 °C, notably lower than compared to a car equipped with a commercial car cover (39.3 °C) and an uncovered car (44.5 °C) (Figure S8c and Figure S8d, Supporting Information), further highlighting its practical application potential. The radiative cooling performances of the membranes are gauged via infrared thermography as the simulated solar irradiation time increased. The BST@TPU membrane consistently maintains lower surface temperatures throughout extended illumination, attributable to its superior solar reflectance in comparison to the TPU membrane (Figure 4e), confirming that the heat generated from BST's UV absorption does not substantially raise its temperature.

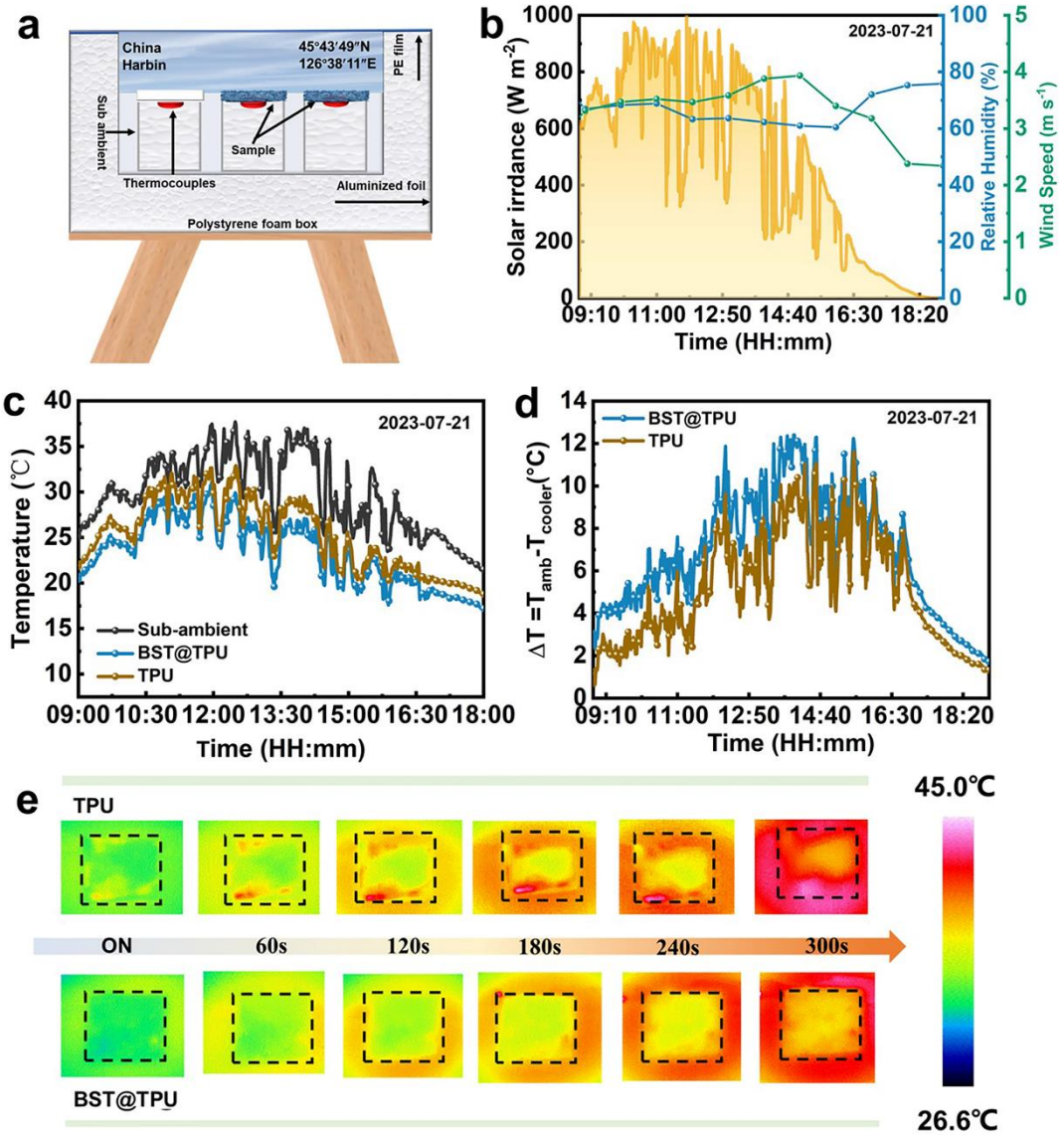

Figure 4. Radiative cooling performances of BST NRs/TPU composite membrane. a) Schematic illustration of the assessment device, the thermocouple is placed under the white foam tank to avoid being heated by direct sunlight. b) Solar irradiance, relative humidity, and wind speed data of the outdoor test environment (Harbin, 45°43′49″N, 126°38′11″E, China, July 21st 2023, 09:00 – 18:00). c) Real-time temperature curves of the outdoor experiment with the TPU membrane and BST@TPU membrane, d) The temperature difference (ΔT=T_{cooler} - T_{amb}) curves of the data in c). e) Surface thermal infrared images of the TPU (3 cm × 3 cm) membrane and BST@TPU membrane (3 cm × 3 cm) under different simulated solar irradiation (xenon lamp) times.

2.5. UV durability of the membranes

To highlight the enhanced UV durability of the BST@TPU membrane, an accelerated aging test was conducted for 216 h under 0.7 kW m^{-2} UV irradiation. The optical performances,

macroscopic color, and microstructure of the membranes were systematically documented. Changes in the reflectivity curves of the TPU membrane and BST@TPU membrane under extended UV irradiation confirm the key role of BST NRs in bolstering the UV durability of TPU (**Figure 5**a). The prolonged UV exposure led to a red shift in the reflective edge of the TPU membrane, indicative of the reduced reflectivity due to its progressive yellowing (Figure S9, Supporting Information). After 72 h UV exposure, the reflectivity of the TPU membrane drops below 90% (Figure S11, Supporting Information). Conversely, the BST@TPU membrane exhibits minimal alterations in its reflectance even after 144 h UV irradiation (Figure S10, Supporting Information). Following 216 h of UV exposure, the BST@TPU membrane retains a reflectivity of 92.1%, while the TPU membrane's reflectivity declines to 84.2% (Figure 5a). At an irradiation power of 0.7 kW h^{-1} in Heilongjiang, a 216 h UV exposure is equivalent to 144 days, representing continuous outdoor exposure throughout the entire summer (Supplementary Note 2.6). The decline in reflectivity substantially impacts the daytime radiative cooling capacity. As shown in Figure 5b, after a 216 h UV aging irradiation, the TPU membrane exhibits a maximum theoretical net radiative cooling power of −0.42 W m^{-2}, indicating a complete loss of radiative cooling capacity due to its low reflectance. In contrast, the BST@TPU membrane maintains a theoretical net radiative cooling power of 85.78 W m^{-2} under identical aging conditions. Notably, minimal changes are observed in the emission characteristics of the membranes, even after UV irradiation (Figure S12, Supporting Information).

Chromaticity variations in the membranes were monitored at 24 h intervals, served as a metric for assessing UV durability. The TPU membrane exhibits a noticeable yellowish hue with extended UV exposure. In contrast, the BST@TPU membrane shows minimal yellowing even after 216 h UV exposure (Figure S13, Supporting Information). A comparison of Figure 5c with Figure 5d highlighted that after 216 h UV exposure, the BST@TPU membrane demonstrates a marginal yellowing effect, registering a Δb^* is 7.35. In stark contrast, the TPU membrane displays a pronounced increase in yellowness, approximately 10 times higher than the BST@TPU membrane. The yellowing is also accompanied by a significant reduction of its structural integrity, as shown by the fracturing of the fibers on the surface of the TPU membrane under a 2 N external force following 216 h of UV aging. In contrast, the BST@TPU membrane withstands the same tensile forces, preserving its mechanical robustness. Notably, the BST@TPU membrane maintains its tensile strength and elongation at break even after enduring 144 h of UV exposure. Extending the UV exposure to 216 h, the elongation of the BST@TPU membrane persists at nearly half (49.6%) of its original value, whereas the TPU membrane

exhibits a marked degradation in the mechanical attributes (Figure 5e and Figure S14, Supporting Information). The integration of BST NRs into TPU not only boosts its UV durability but also preserves its optical properties for outdoor radiative cooling. Density Functional Theory (DFT) calculations unveils that robust adsorption of NH· radicals by BST NRs, originating from the breakage of TPU's C−N bond.[26c, 26d, 35] Remarkably, the O atom exhibits the strongest adsorption energy with NH· (−2.94 eV) (Figure S15, Supporting Information) compared to the free energy of the self-yellowing reaction (−1.27 eV), confirming that the addition of BST NRs effectively captures NH· radicals, interrupting the self-aging reactions and preventing yellowing in TPU (Figure 5f). Under synchronous solar irradiation, typical nitrogen-containing free radical signals (g = 2.000) are captured in electron paramagnetic resonance (EPR) spectroscopy, with an average separation of approximately 11 Gauss between the symmetric, closely positioned twin peaks. [36] A significant reduction in the signal intensity of nitrogen-containing free radicals is observed in the BST@TPU membrane, further confirming the presence of capture constraints between BST NRs and NH· (Figure 5g). Additionally, C1S HRXPS spectra post-irradiation further showcased a reduction in the C−N peak's intensity, emphasizing the role of BST NRs in increasing the UV resistance of TPU (Figure S16, Supporting Information). The negative charge on BST enables electrostatic adsorption with positive NH· radicals, enhancing UV absorption and blocking further UV penetration (Figure S17, Supporting Information). Consequently, BST NRs can not only block UV radiation, but also capture UV-induced free radicals in TPU, subsequently inhibiting the transmission of these free radicals and retarding the aging process of TPU (Figure 5h).

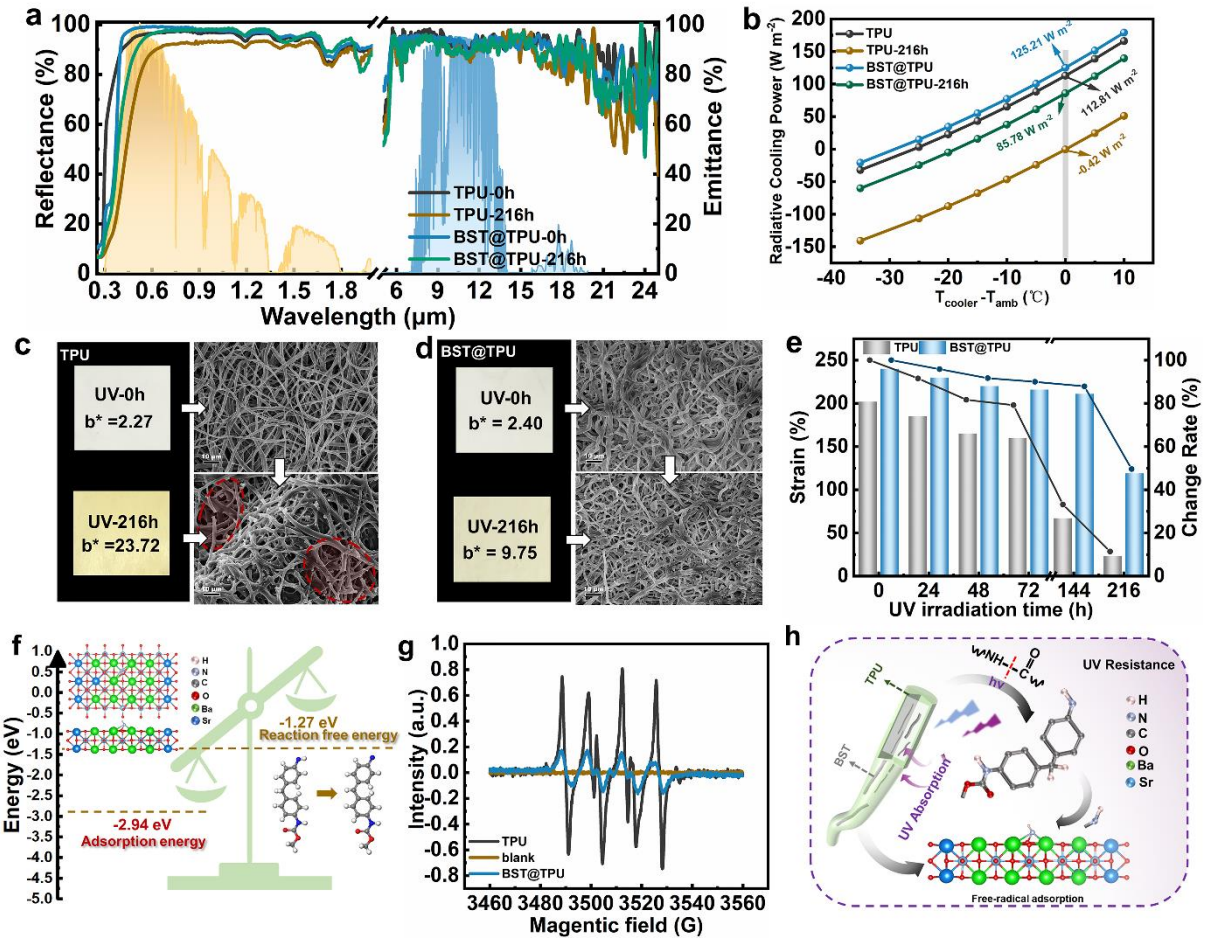

Figure 5. UV durability of the BST@TPU membrane. a) The UV–vis–IR reflectance and IR emittance of TPU membrane and BST@TPU membrane before and after 216 h UV irradiation presented against the AM1.5 solar spectra (yellow) and the atmospheric transparency window (blue). b) Theoretical net radiative cooling power of the TPU membrane and BST@TPU membrane under different UV irradiation times (T_{amb} = 303 K, h_{cc} = 12 W m^{-2}). Optical photographs and SEM images of c) TPU membrane and d) BST@TPU membrane before and after 216 h UV irradiation. e) Strain changes of the TPU membrane and BST@TPU membrane under different UV irradiation times. f) DFT calculations of the adsorption energy and reaction free energy. g) EPR spectra of the TPU and BST@TPU membrane under simulated solar irradiation. h) Schematic diagram of the aging process of TPU and the mechanism of BST NRs for improving the UV durability of TPU.

3. Conclusion

In summary, we have successfully developed a novel core-shell-structured BST@TPU membrane with remarkable UV durability and radiative cooling properties using the coaxial electrospinning technique. BST NRs effectively dispersed the UV radiation on TPU, preventing the accumulation of UV-induced sustained damage. Additionally, BST NRs demonstrate the

capability to capture the NH· generated in TPU due to UV exposure, thereby impeding the aging reactions. Moreover, owing to its high refractive index, BST NRs enhance the scattering of visible light, ensuring high overall reflectance of the TPU membrane. Consequently, the BST@TPU membrane exhibits excellent spectral response with a solar reflectivity of 97.2% (0.25 − 2.5 μm) and infrared emissivity of 93.2% (8 − 13 μm). It delivers a substantial theoretical net radiative cooling power of 125.21 W m^{-2}, leading to a maximum temperature reduction of 12.4 °C in an enclosed measurement box. Remarkably, even after 216 h continuous exposure to 0.7 kW m^{-2} UV radiation, the membrane retains a high reflectance of 92.1% and a theoretical net radiative cooling power of 85.78 W m^{-2}, and almost half of its original tensile strength. This research offers a potentially universal strategy for enhancing the UV aging resistance of radiative cooling polymers while maintaining their optical properties and structural integrity, which could contribute to the advancement of the practical application of radiative cooling technologies.

Supporting Information

Supporting Information is available from the Wiley Online Library.

Acknowledgements

We thank the National Key R&D Program of China (2022YFB3902704), the National Natural Science Foundation of China (No. 52072096), and the Natural Science Foundation of Heilongjiang Province (LH2023E034).

Received: ((will be filled in by the editorial staff))
Revised: ((will be filled in by the editorial staff))
Published online: ((will be filled in by the editorial staff))

References

[1] a) J. Mandal, Y. Fu, A. C. Overvig, M. Jia, K. Sun, N. N. Shi, H. Zhou, X. Xiao, N. Yu, Y. Yang, *Science* **2018**, 362, 315; b) A. P. Raman, M. A. Anoma, L. Zhu, E. Rephaeli, S. Fan, *Nature* **2014**, 515, 540; c) J. Mandal, Y. Yang, N. Yu, A. P. Raman, *Joule* **2020**, 4, 1350; d) Y. Chen, R. Liu, J. Luo, *Progress in Organic Coatings* **2022**, 169, 106936.

[2] a) N. N. Shi, C. C. Tsai, F. Camino, G. D. Bernard, N. Yu, R. Wehner, *Science* **2015**, 349, 298; b) C. Cai, W. Chen, Z. Wei, C. Ding, B. Sun, C. Gerhard, Y. Fu, K. Zhang, *Nano Energy* **2023**, 114, 108625; c) Z. Chen, L. Zhu, A. Raman, S. Fan, *Nat Commun* **2016**, 7, 13729; d) X. Zhao, T. Li, H. Xie, H. Liu, L. Wang, Y. Qu, S. C. Li, S. Liu, A. H. Brozena, Z. Yu, J. Srebric, L. Hu, *Science* **2023**, 382, 684.

[3] a) M. Qin, H. Han, F. Xiong, Z. Shen, Y. Jin, S. Han, A. Usman, J. Zhou, R. Zou, *Adv Funct Mater* **2023**, 33, 2304073; b) X. Li, Z. Ding, L. Kong, X. Fan, Y. Li, J. Zhao, L. Pan, D. S. Wiersma, L. Pattelli, H. Xu, *Materials Advances* **2023**, 4, 804.

[4] a) B. Gu, Q. Xu, H. Wang, H. Pan, D. Zhao, *ACS Nano* **2023**, 17, 18308; b) M. Li, C. Lin, K. Li, W. Ma, B. Dopphoopha, Y. Li, B. Huang, *Small* **2023**, 19, e2301159; c) Y. H. Chen, C. W. Hwang, S. W. Chang, M. T. Tsai, K. N. Jayakumaran, L. C. Yang, Y. C. Lo, F. H. Ko, H. C. Wang, H. L. Chen, D. Wan, *Adv Funct Mater* **2023**, 33, 2301924.

[5] a) W. Zou, L. Pattelli, J. Guo, S. Yang, M. Yang, N. Zhao, J. Xu, D. S. Wiersma, *Adv Funct Mater* **2019**, 29, 1808885; b) D. Li, X. Liu, W. Li, Z. Lin, B. Zhu, Z. Li, J. Li, B. Li, S. Fan, J. Xie, J. Zhu, *Nat Nanotechnol* **2021**, 16, 153.

[6] a) C. Park, C. Park, S. Park, J. Lee, J. H. Choi, Y. S. Kim, Y. Yoo, *ChemSusChem* **2022**, 15, e202201842; b) X. Li, Z. Ding, G. E. Lio, J. Zhao, H. Xu, L. Pattelli, L. Pan, Y. Li, *Chemical Engineering Journal* **2023**, 461, 142095; c) Y. Song, Y. Zhan, Y. Li, J. Li, *Solar Energy* **2023**, 256, 151; d) C. Fu, M. Zhu, D. Zhao, L. Yu, Y. Ding, D. Liu, *Solar Energy* **2022**, 245, 322.

[7] a) W. Li, L. Lu, F. Yan, G. Palasantzas, K. Loos, Y. Pei, *Nano Energy* **2023**, 114, 108629; b) W. Feng, Y.-s. Zhang, Y.-w. Shao, T. Huang, N. Zhang, J.-h. Yang, X.-d. Qi, Y. Wang, *European Polymer Journal* **2021**, 145, 110245; c) J. Wu, M. Wang, L. Dong, J. Shi, M. Ohyama, Y. Kohsaka, C. Zhu, H. Morikawa, *ACS Nano* **2022**, 16, 12801.

[8] a) J. Song, W. Zhang, Z. Sun, M. Pan, F. Tian, X. Li, M. Ye, X. Deng, *Nat Commun* **2022**, 13, 4805; b) M.-C. Huang, C.-H. Xue, J. Huang, B.-Y. Liu, X.-J. Guo, Z.-X. Bai, R.-X. Wei, H.-D. Wang, M.-M. Du, S.-T. Jia, Z. Chen, Y. Lai, *Chemical Engineering Journal* **2022**, 442, 136239; c) S. Zeng, S. Pian, M. Su, Z. Wang, M. Wu, X. Liu, M. Chen, Y. Xiang, J. Wu, M. Zhang, Q. Cen, Y. Tang, X. Zhou, Z. Huang, R. Wang, A. Tunuhe, X. Sun, Z. Xia, M. Tian, M. Chen, X. Ma, L. Yang, J. Zhou, H. Zhou, Q. Yang, X. Li, Y. Ma, G. Tao, *Science* **2021**, 373, 692; d) Q. Zhang, T. Xue, Y. Lu, L. Ma, D. Yu, T. Liu, W. Fan, *Journal of Materials Science & Technology* **2023**, DOI: 10.1016/j.jmst.2023.07.011; e) K. Lin, S. Chen, Y. Zeng, T. C. Ho, Y. Zhu, X. Wang, F. Liu, B. Huang, C. Y. Chao, Z. Wang, C. Y. Tso, *Science* **2023**, 382, 691.

[9] a) P. Yao, Z. Chen, T. Liu, X. Liao, Z. Yang, J. Li, Y. Jiang, N. Xu, W. Li, B. Zhu, J. Zhu, *Adv Mater* **2022**, 34, e2208236; b) Z. Zhang, R. Tian, P. Zhang, C. Lu, X. Duan, *ACS Cent Sci* **2020**, 6, 771; c) D. C. Miller, M. D. Kempe, M. T. Muller, M. H. Gray, K. Araki, S. R. Kurtz, *Progress in Photovoltaics: Research and Applications* **2016**, 24, 1385; d) C. Li, Z. Li, X. Ren, *Colloids and Surfaces A: Physicochemical and Engineering Aspects* **2019**, 577, 695.

[10] H. Aglan, M. Calhoun, L. Allie, *J Appl Polym Sci* **2008**, 108, 558.

[11] a) M. M. Hasan, M. S. Hossain, M. D. Islam, M. M. Rahman, A. S. Ratna, S. Mukhopadhyay, *ACS Appl Mater Interfaces* **2023**, 15, 32011; b) M. Zhou, G. Wan, G. Wang, T. Wieme, M. Edeleva, L. Cardon, R. D'Hooge D, *ACS Appl Mater Interfaces* **2023**, 15, 45300.

[12] B. Zhong, Y. Tang, Y. Chen, Y. Luo, Z. Jia, D. Jia, *Polymer Degradation and Stability* **2023**, 211, 110337.

[13] a) Q. Yue, L. Zhang, C.-Y. He, B.-H. Liu, W.-M. Wang, Z.-W. Lu, G. Liu, X.-H. Gao, *Journal of Materials Chemistry A* **2023**, 11, 3126; b) S. Liu, C. Sui, M. Harbinson, M. Pudlo, H. Perera, Z. Zhang, R. Liu, Z. Ku, M. D. Islam, Y. Liu, R. Wu, Y. Zhu, J. Genzer, S. A. Khan, P. C. Hsu, J. E. Ryu, *Nano Lett* **2023**, 23, 7767; c) C. Fan, Y. Zhang, Z. Long, A. Mensah, Q. Wang, P. Lv, Q. Wei, *Adv Funct Mater* **2023**, 33,

2300794; d) B. Zhu, W. Li, Q. Zhang, D. Li, X. Liu, Y. Wang, N. Xu, Z. Wu, J. Li, X. Li, P. B. Catrysse, W. Xu, S. Fan, J. Zhu, *Nat Nanotechnol* **2021**, 16, 1342.

[14] a) S. Liang, M. Wang, W. Gao, H. Diao, J. Luo, *ACS Omega* **2022**, 7, 25244; b) Z. Tong, J. Peoples, X. Li, X. Yang, H. Bao, X. Ruan, *Materials Today Physics* **2022**, 24, 100658; c) Z. Cheng, H. Han, F. Wang, Y. Yan, X. Shi, H. Liang, X. Zhang, Y. Shuai, *Nano Energy* **2021**, 89, 106377.

[15] a) C. R. Fu, M. Zhu, D. Zhao, L. Yu, Y. Ding, D. X. Liu, *Solar Energy* **2022**, 245, 322; b) C. H. Fan, Y. X. Zhang, Z. W. Long, A. Mensah, Q. Q. Wang, P. F. Lv, Q. F. Wei, *Adv Funct Mater* **2023**, 33, 2300794.

[16] a) Y. Jiang, K. Dong, J. An, F. Liang, J. Yi, X. Peng, C. Ning, C. Ye, Z. L. Wang, *ACS Appl Mater Interfaces* **2021**, 13, 11205; b) J. Xu, H. Nagasawa, M. Kanezashi, T. Tsuru, *ACS Omega* **2021**, 6, 1370.

[17] D. M. King, X. Liang, C. S. Carney, L. F. Hakim, P. Li, A. W. Weimer, *Adv Funct Mater* **2008**, 18, 607.

[18] K. Liu, L. Mi, H. Wang, X. Xiong, K. Zhang, B. Wang, *Ceramics International* **2021**, 47, 22055.

[19] P. Katangur, P. K. Patra, S. B. Warner, *Polymer Degradation and Stability* **2006**, 91, 2437.

[20] X. Shan, L. Liu, Y. Wu, D. Yuan, J. Wang, C. Zhang, J. Wang, *Adv Sci (Weinh)* **2022**, 9, e2201190.

[21] X. Zhang, W. Yang, Z. Shao, Y. Li, Y. Su, Q. Zhang, C. Hou, H. Wang, *ACS Nano* **2022**, 16, 2188.

[22] a) X. Meng, Z. Chen, C. Qian, Z. Song, L. Wang, Q. Li, X. Chen, *ACS Appl Mater Interfaces* **2023**, 15, 2256; b) B. Gu, F. Fan, Q. Xu, D. Shou, D. Zhao, *Chemical Engineering Journal* **2023**, 461, 141919.

[23] Z. Sun, E. Zussman, A. L. Yarin, J. H. Wendorff, A. Greiner, *Advanced Materials* **2003**, 15, 1929.

[24] X. Zhang, S. S. Lv, X. C. Lu, H. Yu, T. Huang, Q. H. Zhang, M. F. Zhu, *Nano Energy* **2020**, 75, 104894.

[25] Z. Shao, X. Zhang, J. Liu, X. Liu, C. Zhang, *Small Methods* **2023**, 7, e2300701.

[26] a) C. Hekimoglu, N. Anil, *J Oral Rehabil* **1999**, 26, 745; b) A. Boubakri, N. Guermazi, K. Elleuch, H. F. Ayedi, *Mat Sci Eng a-Struct* **2010**, 527, 1649; c) A. Ludwick, H. Aglan, M. O. Abdalla, M. Calhoun, *J Appl Polym Sci* **2008**, 110, 712; d) V. Rek, M. Bravar, *Journal of Elastomers & Plastics* **2016**, 15, 33.

[27] W. Luo, L. Xu, G. Zhang, L. Zhou, H. Li, *Composites Science and Technology* **2021**, 204, 108628.

[28] L. Yin, F. Jiang, G. Feng, C. Wu, J. Tan, Q. Wu, R. Zhang, W. Jiang, *Ceramics International* **2022**, 48, 28274.

[29] Y. Lu, X. Xiao, J. Fu, C. Huan, S. Qi, Y. Zhan, Y. Zhu, G. Xu, *Chemical Engineering Journal* **2019**, 355, 532.

[30] a) D. Miao, X. Wang, J. Yu, B. Ding, *Adv Funct Mater* **2021**, 31, 2008705; b) A. Aili, Z. Y. Wei, Y. Z. Chen, D. L. Zhao, R. G. Yang, X. B. Yin, *Materials Today Physics* **2019**, 10, 100127.

[31] a) Z. Ding, L. Pattelli, H. Xu, W. Sun, X. Li, L. Pan, J. Zhao, C. Wang, X. Zhang, Y. Song, J. Qiu, Y. Li, R. Yang, *Small* **2022**, 18, e2202400; b) W. Xie, C. Xiao, Y. Sun, Y. Fan, B. Zhao, D. Zhang, T. Fan, H. Zhou, *Adv Funct Mater* **2023**, 33, 2305734.

[32] Y. Sun, Y. Ji, M. Javed, X. Li, Z. Fan, Y. Wang, Z. Cai, B. Xu, *Advanced Materials Technologies* **2021**, 7, 2100803.

[33] B. Zhao, M. Hu, X. Ao, N. Chen, Q. Xuan, D. Jiao, G. Pei, *Applied Energy* **2019**, 252, 113432.

[34] a) M. I. Iqbal, K. Lin, F. Sun, S. Chen, A. Pan, H. H. Lee, C. W. Kan, C. S. K. Lin, C. Y. Tso, *ACS Appl Mater Interfaces* **2022**, 14, 23577; b) L. Hu, A. Narayanaswamy, X. Chen, G. Chen, *Applied Physics Letters* **2008**, 92.
[35] S. H. Ding, D. Z. Liu, *Construction and Building Materials* **2006**, 20, 878.
[36] a) K. Shirane, *Journal of Polymer Science: Polymer Letters Edition* **2003**, 17, 139; b) L. Hou, Y. Wu, J. Xiao, B. Guo, Y. Zong, *Nuclear Instruments and Methods in Physics Research Section B: Beam Interactions with Materials and Atoms* **2019**, 439, 1; c) A. Nowicki, G. Przybytniak, I. Legocka, K. Mirkowski, *Radiation Physics and Chemistry* **2014**, 94, 22.